A light-weight periodic plate with embedded acoustic black holes and bandgaps for broadband sound radiation reduction

Liling Tang, Nansha Gao, Jiali Xu, et al.

Citation: The Journal of the Acoustical Society of America **150**, 3532 (2021); doi: 10.1121/10.0007067
View online: https://doi.org/10.1121/10.0007067
View Table of Contents: https://asa.scitation.org/toc/jas/150/5
Published by the Acoustical Society of America

JASA ARTICLE

A light-weight periodic plate with embedded acoustic black holes and bandgaps for broadband sound radiation reduction

Liling Tang,[1] Nansha Gao,[1] Jiali Xu,[1] Kean Chen,[1] and Li Cheng[2,a)]
[1]School of Marine Science and Technology, Northwestern Polytechnical University, 127 YouYi West Road, Xi'an 710072, China
[2]Department of Mechanical Engineering, The Hong Kong Polytechnic University, Hung Hom, Kowloon, Hong Kong 999077, China

ABSTRACT:
Conceiving lightweight structures with low vibration and sound radiation properties is an important topic. The concept of Acoustic Black Hole (ABH) offers new impetus to tackle this problem. Most existing ABH structures are based on simple ABH cells. Apart from the reduced structural strength, systematic ABH effects occur typically above the cut-on frequency of the ABH element, which is perceived as a bottlenecking problem. To tackle the problem, this paper examines the sound radiation properties of a plate comprising periodically tangled ABH cells. Through combining ABH effects with sub-wavelength bandgaps (BGs), numerical and experimental studies show that the plate exhibits reduced sound radiation properties in an ultra-broad frequency range, far below the cut-on frequency of an ABH element. This is owing to the tangled nature of the ABH elements, which extends the actual dimension of the ABH, lowers its onset frequency and reduces the sound radiation efficiency through creating slow waves. Inside the BGs, the reduced sound radiation is mainly due to the redistribution of the vibration energy, basically confined to the excitation area. Capitalizing on the combined ABH and BG features alongside improved mechanical properties, the proposed structure shows promise as a light-weight solution for broadband noise reduction. https://doi.org/10.1121/10.0007067
(Received 22 June 2021; revised 15 October 2021; accepted 20 October 2021; published online 10 November 2021)
[Editor: Laurent MAXIT] Pages: 3532–3543

I. INTRODUCTION

Efforts for developing lightweight structures with low vibration and sound radiation properties have been persistent in the structural acoustics community, and the topic is of vital importance for a large variety of engineering problems in fields like aerospace and transportation. However, traditional acoustic theory indicates that lightness in structures seems always be in conflict with the demand for lower vibration and noise, exemplified by the well-known mass law which governs the mid-to-high frequency sound transmission. Sound radiation from thin-walled structures heavily relies on the wave propagation properties of flexural waves and its interaction with the surrounding acoustic medium. Therefore, an effective wave manipulation would greatly benefit the design of light-weight and sound-proofing structures.

Acoustic Black Hole (ABH) effects offer new possibilities to accomplish the aforementioned task. ABH phenomenon stems from the flexural wave propagation properties in a structure with its thickness tailored according to a decreasing power-law function to achieve diminishing phase velocity and energy accumulation along the propagation path.[1,2] The resultant highly focalized energy can then be efficiently dissipated by a small amount of damping layers coated over the vibrating structure. This, alongside the reduced thickness and material removal, also contributes to reducing the overall structural weight compared with conventional uniform structures. Existing research has demonstrated multiple appealing properties of the ABH designs as an effective vibration mitigation measure theoretically[3–8] and experimentally.[9–12]

Compared with the extensive research in vibration, studies of ABH structures for noise control are much less. Among existing works, Bowyer *et al.*[13] experimentally demonstrated that a plate with six ABH indentations can achieve substantial sound radiation reduction as a result of the overall reduction of vibration response. Almost simultaneously, Conlon *et al.*[14] numerically analyzed the physical mechanisms behind the sound radiation reduction in ABH plates through examining modal loss factors. Wavenumber transform method was also used to demonstrate the acoustic decoupling phenomena and the vibration reduction resulting from the ABH effects.[15] Subsequently, Li *et al.*[16] studied the sound radiation of a single one-dimensional ABH beam structure and proposed ways to enhance the interaction between the bending waves and the ABH elements for better low-frequency performance. Ma *et al.*[17] then established a two-dimensional wavelet model to study the sound radiation and transonic boundaries of a plate containing a single ABH, based on which a topological optimization was later proposed to determine the layout of the damping layer to minimize sound radiation.[18] Apart from the aforementioned free-field problems, Ji *et al.*[19] investigated the feasibility of using ABH structures to reduce the interior sound field in a plate-cavity system and explained the underlying mechanism

a)Electronic mail: li.cheng@polyu.edu.hk, ORCID: 0000-0001-6110-8099.

https://doi.org/10.1121/10.0007067

through a vibroacoustic coupling analysis.[20] The potential of ABH structures for sound transmission was also addressed by Feurtado *et al.*[21] and Deng *et al.*[22] from numerical and experimental perspectives. It should be noted that all above research studies focus on basic ABH design which incorporates simple or multiple ABH cells in their primitive form. As such, structures suffer from structural strength problems arising from the thin thickness of the ABH cells. Most importantly, this imposes a low frequency barrier, below which the expected ABH effects can hardly play out systematically. Typically, this frequency barrier for a simple ABH structure is delimited by the so-called cut-on/characteristic frequency of a single ABH cell which depends on the ABH size.[23] For practical applications, however, noise control in the mid-to-low frequency range is of paramount importance and technically challenging. Efforts have been made in improving low-frequency ABH performance from a vibrational perspective through exploiting system nonlinearities to achieve low-to-high frequency energy transfer.[24–26] However, exploration on low-frequency acoustic performance of ABH structures is still scarce. Therefore, the main motivation of this work is to explore possibilities to conceive light-weight ABH structures for better and broadband acoustic performance, especially at low frequencies relative to the conventional cut-on frequency.

While conventional ABH design allows for the manipulation of wave propagation velocity, new concepts like periodic or phononic crystals provide additional means to fundamentally change the wave propagation nature through the creation of bandgaps (BGs) to completely prohibit wave propagation in an infinite lattice. Even when the lattice is truncated into a finite size, vibration energy can still be redistributed over the structure or confined to a certain area in the frequency range corresponding to the BGs, which also plays a vital role in determining the ultimate sound radiation properties of the structure. By embedding periodic one-dimensional (1D) ABH elements into beams or plates, ultra-wide and sub-wavelength BGs have been achieved, which show promise for vibration energy isolation and control.[27–29] Subsequently, various ABH-based designs of periodic structures were reported for vibration reduction purposes.[30,31] We also preliminarily demonstrated that BGs in plates with periodic 1D tunneled ABHs are also beneficial for reducing the sound radiation by lowering the radiation efficiency,[32] but only within narrow and directional BGs. The resultant sound radiation reduction was also quite limited.

To achieve omni-directional BGs for flexural waves, we proposed a plate containing periodical double-layer two-dimensional (2D) ABHs in our previous work.[33] Despite the attractive vibration properties revealed, it is not clear how the complete sub-wavelength BGs would affect the acoustic radiation properties of the structure. Meanwhile, whether the proposed design with tangled ABH elements would bring any acoustic benefit also remains unknown. This constitutes another main motivation of the present work, namely to explore possible acoustic benefits as well as the underlying physics of such periodic plates, empowered with embedded ABH and BGs features.

To this end, this paper examines the sound radiation properties of a plate comprising periodically tangled double-leafed ABH cells. The plate features light-weightiness by tangled holes, improved stiffness by double branched facing, and BGs by the periodic arrangement of the ABH cells. As such, analyses focus on its sound radiation properties and their inherent relationships with ABH features and BG properties. The outline of the paper is as follows. The plate and the analysis method are first introduced. Then, predominant acoustic radiation phenomena, i.e., sound radiation efficiency and radiation sound power, are investigated and compared with a uniform plate. Supersonic intensity and wavenumber analyses are then carried out to reveal underlying mechanisms. Finally, experiments are conducted to validate the observed sound radiation phenomena as well as the reduced sound radiation properties of the designed plate. Conclusions are finally drawn.

II. MODEL AND ANALYSIS METHOD

A. Structure model

Consider a plate composed of $L \times M$ periodically arranged ABH cells, exemplified by an 8×6 cells in Fig. 1(a). The lattice constant and the thickness of the unit cell are a and h, respectively. Seen from outside, the plate resembles a uniform plate, with flat surface outside but hollow structure inside (depicted by dark gray area), as sketched in Fig. 1(b). The inner structure of the unit cell excised by a quarter is displayed in Fig. 1(c). Each unit cell is a uniform plate excavated inside with a symmetrical circular ring, tapered according to an ABH profile. The thickness of the ABH profile is tailored according to $h(x) = \varepsilon(x - r)^m + h_0$ with m being the taper power index, h_0 the residual truncation thickness and r the reserved length, as shown in a cross-sectional view in Fig. 1(d). The radial length of the ABH is l_{ABH}-r. The design philosophy stems from the consideration of wave propagation properties in a 2D ABH plate, mainly from three aspects.[33] These considerations are briefly recapped here for completeness. First, to achieve local resonant BGs, all incoming waves should be forced to pass through or fall into the ABH indentation area through intersection of outer periphery of the ABH and the boundary of the uniform plate element. Therefore, an intersecting condition should be satisfied by $\sqrt{2}l_{\mathrm{ABH}} < a < 2l_{\mathrm{ABH}}$. Second, a cylinder with radius r is used to connect the two branches of the ABH indentation and to create a large impedance mismatch, thus realizing broader BGs through combined local resonances and Bragg scattering. Finally, the double-layer ABH indentation design is adopted to achieve dual benefit: reducing the coupling between the ABH-induced local resonance and the global vibration of the unit cell, which is shown to be conducive to creating broadband BGs, and ensuring better structural integrity and overall strength. Such a design leads to a light-weight plate owing to the periodically tangled double-leaf ABH connections inside the structure.

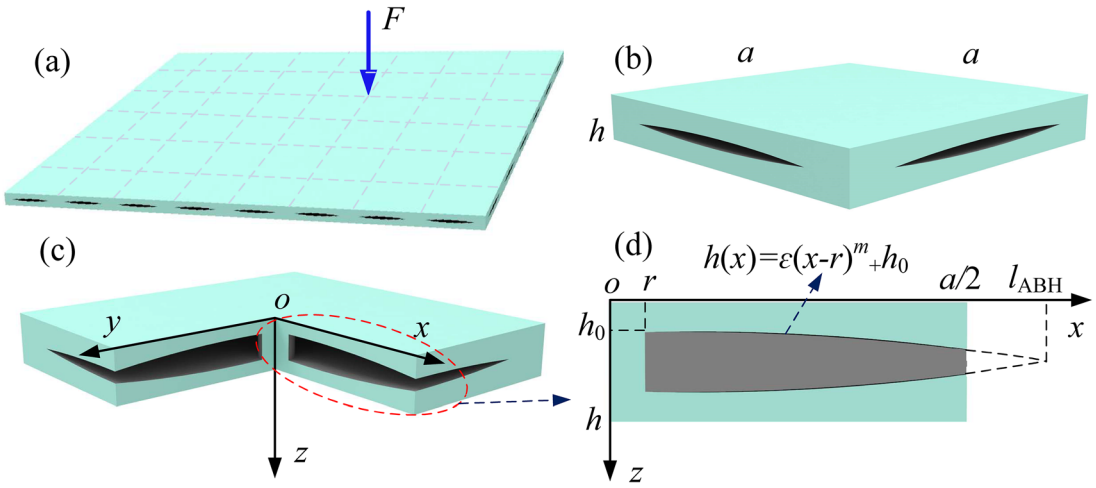

FIG. 1. (Color online) Structure model: (a) a finite plate composed of 8 × 6 cells with a harmonic point force excitation; (b) a unit cell; (c) a unit cell excised by a quarter; (d) local cross section as circled by the red dash line in (c).

COMSOL Multiphsics 5.2 with Solid Mechanics Module is used to calculate the vibration velocity $\boldsymbol{v}$, when the plate is subject to a point excitation force. Considering the sound radiation into a light fluid like air, the fluid loading effects on the plate due to the acoustic radiation are ignored when calculating structural responses. The plate is densely meshed to ensure at least ten elements per wavelength for the highest frequency of interest, i.e.,5000 Hz in present case. Specifically, the plate surface is meshed with equally distributed trilateral elements, compatible with subsequent sound radiation calculation using elementary radiator acoustical model, while the rest is meshed with tetrahedral elements. The whole model consists of 1 013 595 tetrahedral elements. The plates used in the simulation are made of aluminum with a mass density of 2700 kg/m^3, Young's modulus of 70 MPa, Poisson's ratio of 0.3, and damping loss factor of 0.001. The structural parameters are a = 60 mm, h = 5 mm, h_0 = 0.3 mm, m = 4, r = 10 mm, and l_{ABH} = 40 mm. For analyses, the conventionally defined cut-on/characteristic frequency for one single ABH cell is used as an indicative reference, knowing that the current structure with tangled ABH cells is a complex one. This makes it difficult, if not theoretically impossible, to precisely define the actual characteristic dimension 2 l_{ABH} to calculate the corresponding cut-on frequency. Nevertheless, using 2 l_{ABH} = 80 mm, the characteristic frequency for a single ABH cell is estimated at 7564 Hz, as obtained from $f_{\mathrm{Char}} = \pi/(2l_{\mathrm{ABH}})^2\sqrt{Eh^2/3\rho(1-\upsilon^2)}$.[32] Note this frequency is far above the highest frequency of interest, i.e., 5000 Hz. Therefore, the main focus of the present study is on the low frequency range, relative to the conventional cut-on/characteristic frequency of a single ABH cell.

B. Acoustical model

The plate is mounted on an infinite rigid baffle with exclusion of the edge diffraction of acoustic waves. Based on elementary radiator acoustical model,[34] upon obtaining the transverse velocities vector $\boldsymbol{v}$ of each element on the plate surface through the finite element method (FEM), the sound pressure vector can be expressed by using the radiation impedance matrix $\mathbf{Z}$ as

$$\boldsymbol{p} = \mathbf{Z}\boldsymbol{v}, \tag{1}$$

where $Z_{\mathrm{ij}} = j\omega\rho_0 A e^{-jkR_{ij}}/2\pi R_{ij}$ with ρ_0 being the density of air, ω and k the angular frequency and wavenumber, respectively, A the area of each element, and R_{ij} the distance between the ith and jth elements. Then, the total sound power radiated by the plate can be obtained by the summation of the power radiated from each element as

$$W = \sum_{i=1}^{N}\frac{1}{2}A\mathrm{Re}\{v_i^* p_i\} = \frac{A}{2}\mathrm{Re}\{\boldsymbol{v}^{\mathrm{H}}\mathbf{Z}\boldsymbol{v}\} \tag{2}$$

in which * and $^{\mathrm{H}}$ represent complex conjugate and Hermitian transpose, respectively; N is the total number of meshed elements on the plate surface.

The sound radiation efficiency of the plate is used as the key metric to quantify the sound radiation properties of the plate, which is defined as

$$\sigma = \frac{W}{\rho_0 c_0 S\langle\overline{v^2}\rangle}, \tag{3}$$

where c_0 is the sound speed; $\langle\overline{v^2}\rangle$ is the average mean square velocity over the whole vibration surface, which can be expressed in present case as $\langle\overline{v^2}\rangle = (A/2S)\boldsymbol{v}^{\mathrm{H}}\boldsymbol{v}$ with S being the total area of the vibration surface.

In the calculation, the density ρ_0 and the sound speed c_0 of air are set to be 1.21 kg/m^3 and 343 m/s, respectively. The critical frequency f_c of the corresponding uniform plate is 2430 Hz, calculated by

$$f_c = \frac{c_0^2}{2\pi}\sqrt{\frac{12\rho(1-\upsilon^2)}{Eh^2}}. \tag{4}$$

Above f_c flexural waves bear wavelengths larger than those of the radiated acoustic waves in air and they are supersonic and efficient in sound radiation.

https://doi.org/10.1121/10.0007067

C. Analysis method

Supersonic intensity[35] and wavenumber analyses[15] will be employed in due course to analyze the underlying mechanisms, which are briefly introduced hereafter.

In comparison with classical acoustic intensity, supersonic intensity, by filtering out the subsonic wave components, allows direct identification of regions which dominate the sound radiation to reach far field.[36] The supersonic intensity is defined as

$$I^{(s)}(x,y) = \frac{1}{2}\mathrm{Re}\left\{p^{(s)}(x,y)v^{(s)}(x,y)^*\right\}, \tag{5}$$

where $p^{(s)}$ and $v^{(s)}$ are the supersonic pressure and velocity, respectively, which can be obtained as[37]

$$p^{(s)}(x,y) = p(x,y) * h^{(s)}(x,y), \tag{6}$$

$$v^{(s)}(x,y) = v(x,y) * h^{(s)}(x,y), \tag{7}$$

in which * denotes the two-dimensional convolution operator, $h^{(s)}(x,\ y)$ is the filter function of subsonic waves, expressed as $h^{(s)}(x,y) = \left(k/2\pi\sqrt{x^2+y^2}\right)J_1\left(k\sqrt{x^2+y^2}\right)$ with J_1 being the Bessel function of the first kind.

Wavenumber spectra decompose the vibration field into different wavenumber components with the amplitude showing the energy distribution in supersonic and subsonic waves. Therefore, these features can be exploited here to understand the sound radiation mechanisms of the ABH structures.

Specifically, the velocity field $v(x,y,f)$ in the spatial domain can be transformed into wavenumber domain through a two-dimensional Fourier transform as

$$V(k_x,k_y,f) = \int\int v(x,y,f)e^{-jk_x x}e^{-jk_y y}dxdy, \tag{8}$$

with k_x and k_y being the wavenumbers in the x and y directions, respectively.

III. RESULTS AND DISCUSSIONS

A. Acoustic radiation performance

Numerical simulations first demonstrate the superior sound radiation properties of the proposed plate in terms of sound radiation efficiency, σ, (σ_{ABH} for ABH panel and σ_u for uniform panel) in a baffled infinite free space for two different boundary conditions, as shown in Fig. 2. Results from a uniform plate of the same thickness and dimension are also included for comparisons. For the free plates, Fig. 2(a) shows that ABH plate exhibits a generally lower σ than its uniform counterpart, except at the very low frequency range and inside the marked shadow area where both panels show very similar σ. More specifically, σ_{ABH} is systemically lower than σ_u before 1100 Hz with a maximum reduction up to nearly 20 dB. Then, σ_{ABH} experiences a sudden increase to approach the same level as the uniform plate, roughly from nearly 1100 to 2400 Hz, which corresponds exactly to the BG obtained from the analysis on the corresponding infinite periodic ABH plate (marked by gray area). Note the broadband BG is obtained by examining the band structures of a unit cell under Floquet-Bloch periodic boundary conditions and by using a parametric sweep of the reduced wave vector $k\pi/a$ over the first irreducible Brillioun zone, details of which can be found in our pervious paper.[33] Above the BG, while σ_u shows an upward trend when approaching and exceeding the critical frequency of the panel (2430 Hz in the present case), σ_{ABH} on the contrary reduces in the same region. As a result, σ_{ABH} is again significantly reduced compared with the uniform one, resulting in an overall reduction of around 10 dB. The same analysis is repeated for the clamped boundary condition, as shown in Fig. 2(b). Albeit some differences in levels, the general variation trends of σ in relation to the two types of panels, is very similar to the previous free-boundary case. In addition, an obvious reduction in σ_{ABH} inside the BG is also observed. Despite the sudden rise within the BG, σ_{ABH} is generally lower than σ_u above 190 Hz. Since the radiation efficiency measures the sound radiation capability of a structure in radiating sound

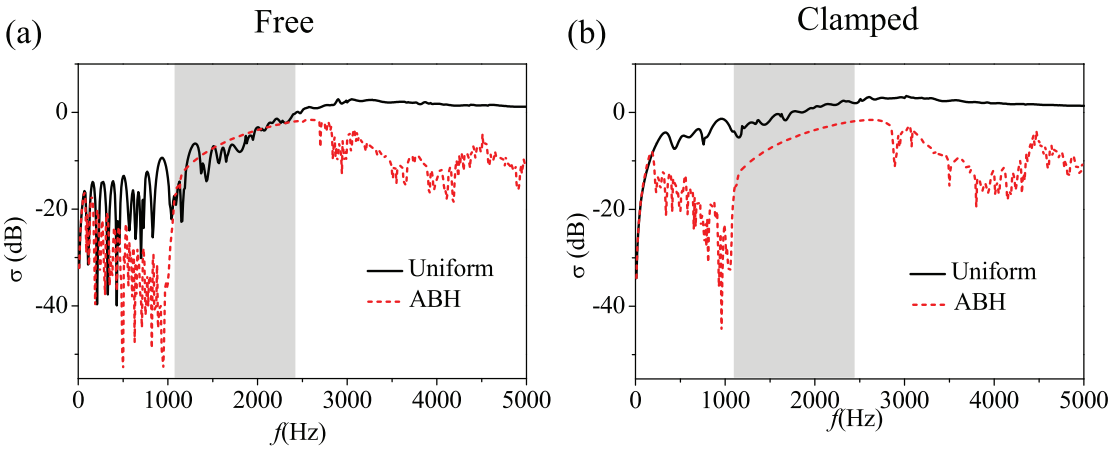

FIG. 2. (Color online) Sound radiation efficiencies of the periodic ABH plates compared with their uniform counterparts under free (a) or clamped (b) boundary conditions.

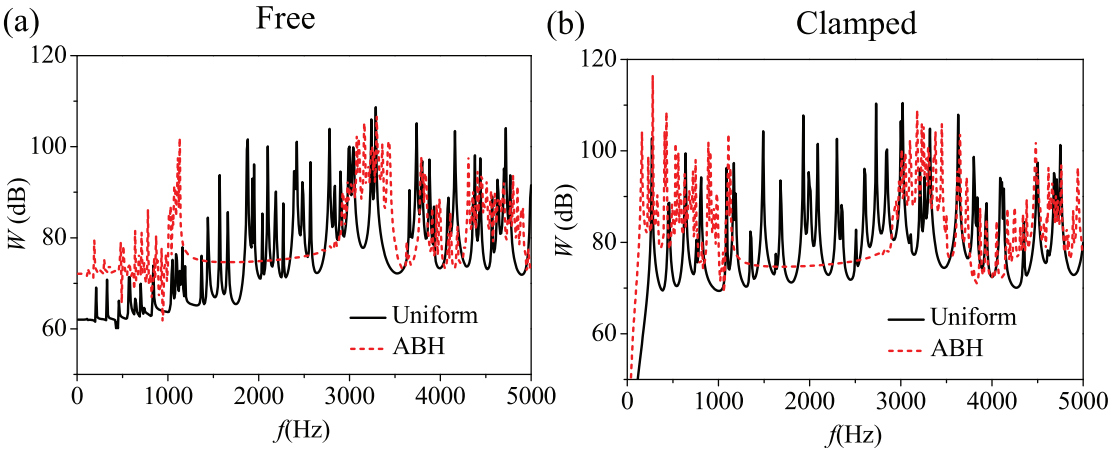

FIG. 3. (Color online) Radiation sound power comparison between the periodic ABH plate and the counterpart uniform plate under free (a) or clamped (b) boundary conditions.

into the far field for the same given amount of vibration energy, the above observation demonstrates the superior sound radiation properties of the proposed ABH panels. The observed systematic and broadband reduction in the sound radiation efficiency of the proposed periodic ABH plate indicates that its acoustic radiation ability is remarkably weakened compared with its uniform counterpart, and this phenomenon starts from low frequencies which are far below the cut-on/characteristic frequency of a single ABH cell. Moreover, the ABH plates also stand out by their light weight: 31% the mass and 54% the stiffness of the uniform plate in the present case. Note the so-called stiffness refers to the equivalent overall bending stiffness, which can be obtained by integrating the sectional bending stiffness EI over the whole plate, with I being the inertia moment. This indeed evidences the light-weight feature of the design and, albeit reduced, can still offer acceptable structural stiffness, which can hardly be achieved by conventional ABH design.

Figure 3 further compares the radiated sound power from the ABH plate and the uniform plate under a unit harmonic force excitation at the arrow position shown in Fig. 1(a) for the same two sets of boundary conditions examined above. Interesting is that different from radiation efficiency, the radiation sound power of the ABH plate is significantly reduced compared with the uniform plate within the BG for both cases, with the maximum reduction reaching up to more than 30 dB. Note the BG is far below the cut-on/characteristic frequency of a single ABH cell, i.e., 7564 Hz. Therefore, with only one third of the mass and in the absence of damping layers, systematic and significant reduction in the radiated sound power can be achieved at relatively low frequencies far below the characteristic frequency of a single ABH cell through achieving broadband sub-wavelength BGs. However, outside the BG, although σ is systematically reduced, the radiation sound power of the ABH plate is comparable with or even larger than that of the uniform plate, due to the assumption of the constant input force.

To further verify the above, a comparison is made based on constant input power instead of constant input force. Note in practice, the real input force depends on the interaction between the driving element and the receiving structure. As a result, due to the differences in the reacceptance of the two plates, energy input into the two plates can be very different. Therefore, the above comparison is re-examined by normalizing the radiated sound power to the input power, $\mathrm{Re}\{Fv^*\}$ for each plate. Results are shown in Fig. 4, which demonstrates that the normalized radiated power of the ABH plate is systematically lower than that of the uniform plate over almost the entire frequency range, again for both types of boundaries. The reduction inside the BG is particularly remarkable, amounting to 40 dB. This further confirms the superior ability of the proposed periodic ABH plate in reducing acoustic radiation over broadband, including low frequencies far below the cut-on/characteristic frequency of a single ABH element.

B. Underlying mechanisms

To reveal the mechanisms underpinning the observed low sound radiation properties of the periodic ABH plates, analyses are conducted using wavenumber analyses and supersonic intensity with comparisons with the corresponding uniform plates at selected representative frequencies, i.e., outside and inside the BG, respectively. Without loss of generality, plates with free boundary under a unit force excitation are used in analyses.

1. ABH effects outside BG

Outside the BG, exemplified by 950 Hz, the transverse velocity distribution over the plates (both uniform and ABH) are compared in Figs. 5(a) and 5(b). It follows that the vibration energy is spread out over the ABH plate with a level, which is typically four orders of magnitude higher than that of the uniform plate. The significant increase in the vibration level on the ABH plate can be attributed to the reduction in mass by 70.9% and in bending stiffness by 46%, as compared with its uniform counterpart. Despite the high vibration level, its sound radiation efficiency, σ_{ABH}, is

https://doi.org/10.1121/10.0007067

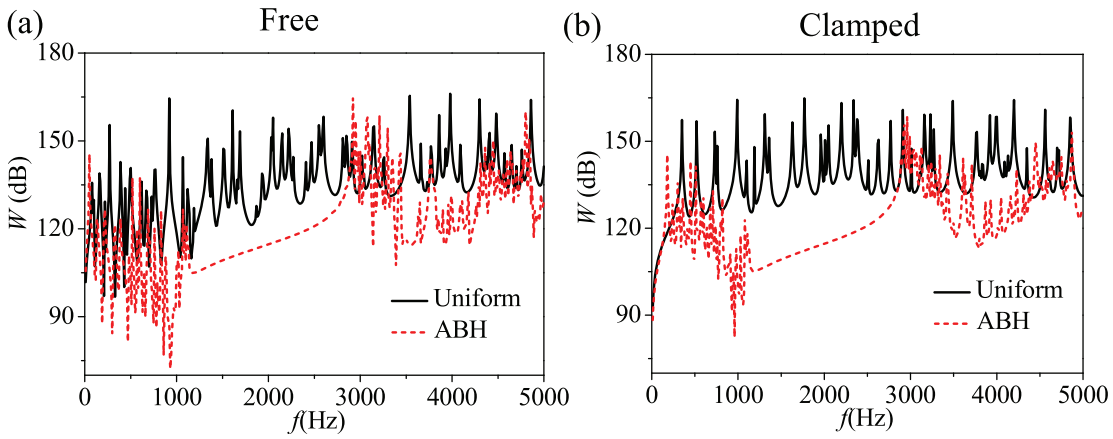

FIG. 4. (Color online) Comparison of radiated sound power per unit input power between the periodic ABH plates and uniform plates under free (a) or clamped (b) boundary conditions.

reduced oppositely as shown in Fig. 2. To reveal the underlying mechanisms, corresponding wavenumber spectra of the square of the wavenumber transform of the velocity are displayed in Figs. 5(c) and 5(d), with amplitudes presenting the energy distribution in the wavenumber domain. A radiation circle is also included as reference, along which the acoustic wavenumber equals to the structural wavenumber, i.e., $k_x^2 + k_y^2 = k_c^2 = (2\pi f/c_0)^2$ with k_c being the acoustic wavenumber. Within this circle, structural wave components are supersonic, which efficiently radiate sound into the far field. Outside the circle, energy components are subsonic with much reduced sound radiation ability to the far field. Figure 5(c) shows that the uniform plate mainly contains subsonic vibration energy components around and outside the radiation circle. This is because 950 Hz is below the critical frequency of 2430 Hz. Nevertheless, the sound radiation efficiency is still relatively high albeit less than 1 [shown in Fig. 2(a)], as compared to the ABH plate. In fact, as shown in Fig. 5(d), high energy components of the ABH plate are spread out to higher wavenumber domain outside the radiation circle. As a result, the energy from supersonic components inside and around the radiation circle is much lower than that of the uniform plate, as shown in Figs. 5(c) and 5(d), also confirmed by Fig. 2(a). The observed super-to-subsonic wavenumber transformation is due to the ABH-induced wave phase velocity reduction.

Interesting is that the effective ABH frequency is far below the cut-on/characteristic frequency of an ABH

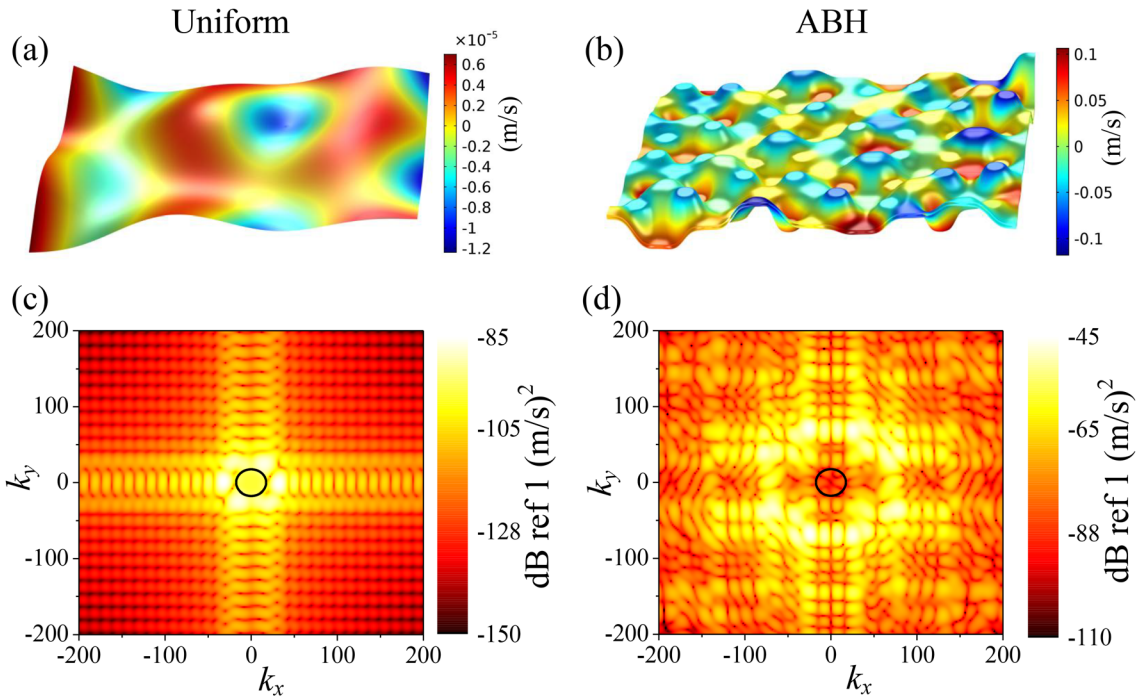

FIG. 5. (Color online) (a), (b) Velocity distribution, and (c), (d) wavenumber spectra comparison between the uniform plate and ABH plate at $f = 950$ Hz below the BG, with solid line denoting the radiation circle.

element. As further evidence of the early onset of the ABH effects, the modal loss factors of the plates are shown in Fig. 6, after the whole outside surfaces are covered by damping layers with a thickness $h_d = 0.3$ mm. The damping layers are made of 3M^{TM} VHB^{TM} F9473PC with a mass density of 980 kg/m^3, Young's Modulus of 30 MPa, Poisson ratio of 0.499, and damping loss factor of 0.9. As can be seen, with the deployment of the damping layers, the modal loss factors of the ABH plate significantly increase even for the lower-order modes, in drastic contrast to the quasi-invisible increase in the uniform plate. This is due to the ABH-induced energy concentration and the subsequent effective dissipation, as evidenced by the typical local ABH mode shape shown in Fig. 6. This systematic increase in the modal loss factors, starting from lower-order modes, is totally different from the previous research based on conventional ABH designs.[5,6,14]

It is obvious that the ABH plate and the uniform plate used above have different overall mass and stiffness. As an attempt to eliminate these effects for a fair comparison, a uniform plate with the same equivalent stiffness and mass as the ABH plate is examined, whose loss factors are also included for comparison (shown by blue triangles) in Fig. 6. Clearly the corresponding modal loss factors are also much less than that of the ABH plate in the entire frequency range. This suggests that the aforementioned damping enhancement is indeed due to the onset of the ABH effect, rather than the reduced structural stiffness and mass. Corresponding wavenumber transformation from supersonic to subsonic at low frequencies in the presence of damping materials (not included here) also confirms this. To further demonstrate the earlier cut-on of the ABH effects, Fig. 7 shows a comparison in terms of σ between the ABH plate and the uniform plate with equivalent stiffness and mass. The equivalent uniform plate resembles the original uniform plate in that its σ is also systematically higher than that of the ABH plate, including the low frequencies. This echoes the above observation that the sound radiation efficiency reduction at low frequencies results from the earlier cut-on

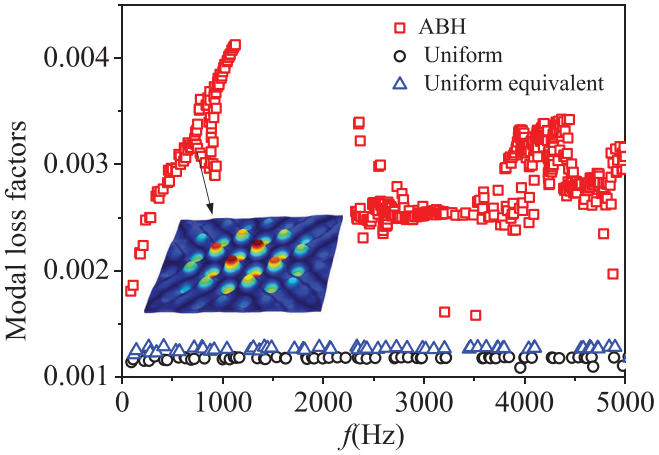

FIG. 6. (Color online) Structural modal loss factors with damping layers applied.

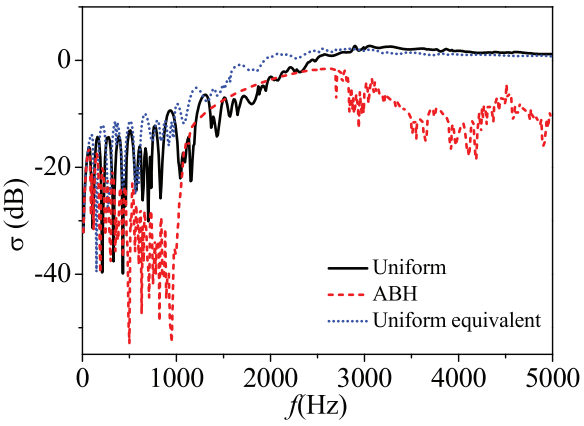

FIG. 7. (Color online) Sound radiation efficiency comparison between the ABH plate and the uniform plate with equivalent stiffness and mass.

of ABH effect instead of the effect from reduced mass and stiffness. In fact, the tangled nature of the ABH elements arising from the special design significantly extends the actual characteristic dimension of the ABH. As a result, the ABH is effective at lower frequencies and therefore reduces the sound radiation efficiency by creating slow waves inside the structure, even at quite low frequencies.

The same analysis is conducted for frequencies above the BG, exemplified by 4190 Hz. The wavenumber spectra are shown in Fig. 8, again for the two plates. Since the frequency is now above the critical frequency, most vibration components of the uniform plate are supersonic and located inside the radiation circle [shown in Fig. 8(a)], radiating far field sound power effectively with a σ approaching one. In contrast, Fig. 8(b) shows that ABH plate contains much reduced supersonic energy components inside the radiation circle. In fact, the contrast between the reduced energy level inside the radiation circle and the increase outside testifies the typical structural wave speed transformation process, from supersonic to subsonic, typical of ABH effects.

2. Effects of the bandgap

Within BG, the velocity distribution and the corresponding wavenumber spectra at the representative frequency 1880 Hz are presented in Fig. 9. For the uniform plate, the vibration velocity is rather evenly distributed over the entire plate. However, for the ABH plate, the vibration is only confined to the excitation area with an amplitude level typically four orders of magnitude lower than the uniform plate. The vibration is significantly attenuated when passing through the ABH cells near the excitation because of the BG properties in stopping wave propagation, and can hardly be observed in the rest part of the plate, as shown in Fig. 9(b). This rather singular spatial distribution of the vibration energy over the ABH plate results in a spreading out of the wave numbers, as evidenced by Fig. 9(d), which is quite different from Fig. 9(c) for the uniform plate. It can be seen that, outside the BG, though with a much reduced amplitude, energetic energy components of the ABH plate are inside and around the radiation circle, similar to the

https://doi.org/10.1121/10.0007067

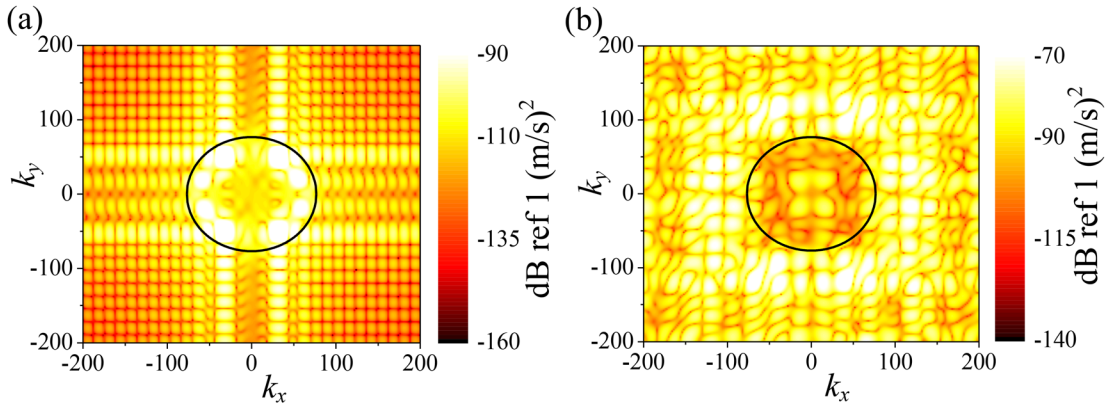

FIG. 8. (Color online) Wavenumber spectra of (a) the uniform plate and (b) the ABH plate at representative frequency $f = 4190$ Hz above the BG, with solid line denoting radiation circle.

uniform plate. This can be understood from two aspects. On one hand, as observed in Fig. 9(b), the BG leads to a redistribution of the vibration energy and its concentration within the excitation area. In the process, the prohibited wave propagation to other ABH cells weakens the wave speed reduction effects of the ABH. On the other hand, the vibration distribution over the plate at the frequencies inside the BG becomes more singular, close to a Dirac function in the extreme case. Therefore, the spatial Fourier transform becomes more broadband in terms of wave numbers, containing more supersonic components. As a result, the sound radiation efficiency is almost at the same level as the uniform plate despite its reduced vibration level, consistent with results shown in Fig. 2(a).

Despite a very similar σ level, the radiated sound power from the ABH plate is much less than that from the uniform plate, as observed before. This obviously cannot be explained from the angle of structural wave speed reduction as discussed before. To better understand this, the corresponding supersonic intensity maps for the two plates are presented in Fig. 10. It can be seen that the maps are consistent with the vibration velocity distribution for each plate. More specifically, while the sound energy is effectively emanated from multiple energetic areas over the uniform plate, in the ABH plate, however, the supersonic intensity is basically confined to the limited excitation area, same as the vibration velocity. With significantly reduced vibration level, averaged over the plate, the magnitude of supersonic intensity is also considerably decreased, so is the radiation sound power.

To demonstrate that the aforementioned features indeed originate from the intrinsic properties of the ABH due to the

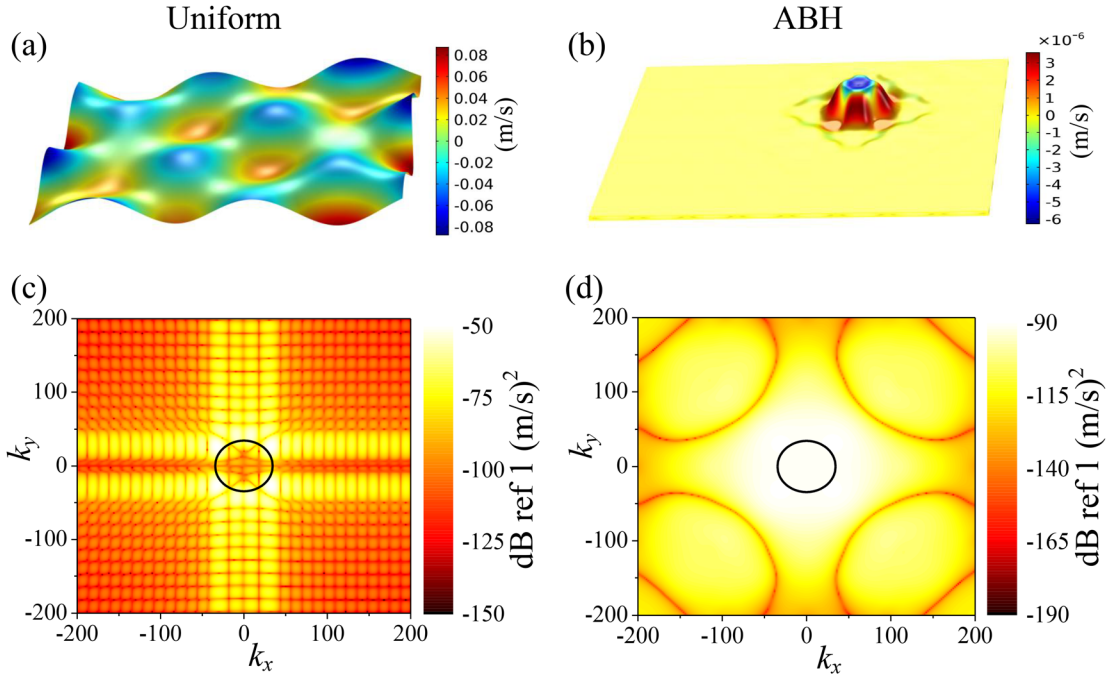

FIG. 9. (Color online) (a), (b) Velocity response and (c), (d) wavenumber spectra comparison between the uniform plate and ABH plate at representative frequency $f = 1880$ Hz within the BG.

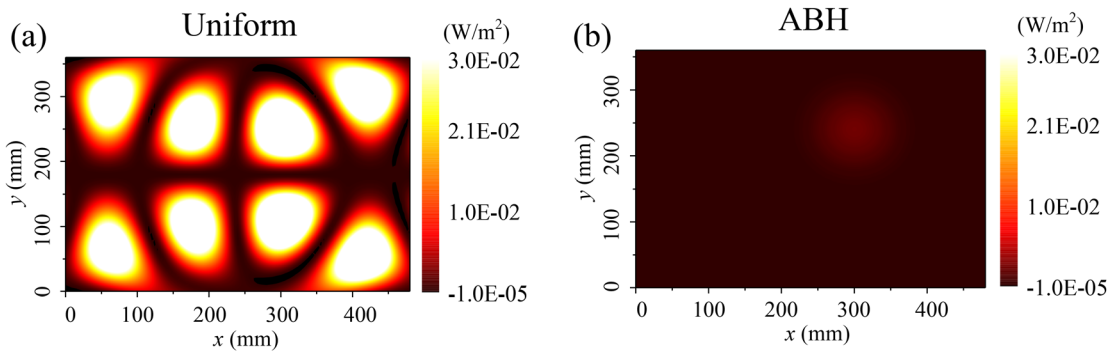

FIG. 10. (Color online) Supersonic intensity of (a) the uniform plate and (b) the ABH plate at representative frequency $f = 1880$ Hz.

power-lawed thickness variation, an extreme case with an infinitely large m is considered. The case degenerates from the nominal ABH case, leading to a structure with a cylindrical cavity between the double walls. It is observed that, although BGs can still be achieved at low frequencies, the total bandwidth is much narrower compared with the present ABH case with $m = 4$. This is because an ABH with an infinite taper power index would break the smoothness criteria, and generate adverse wave reflections at the connection between the uniform and the thinned parts. This jeopardizes the creation of the slow waves, thus adversely impacting on the generation of BGs induced by the combined effect of local resonances and Bragg scattering. Meanwhile, the bandwidth and the radiated sound power reduction are also significantly reduced. This confirms the key role that ABH effect plays in the designed structure which leads to the observed sound radiation reduction.

To sum up, the superior sound radiation properties brought by the designed periodic ABH plate can be attributed to two factors. The ABH-induced wave speed reduction explains the systematic reduction in sound radiation efficiency outside the BG, through transforming supersonic waves to subsonic ones. This takes place at low frequencies far below the cut-on/characteristic frequency of an ABH element. This is attributed to the tangled nature of the ABH elements arising from the design, which extends the effective characteristic dimension of the ABH to lower the ABH effective frequency. Within the BG, however, the reduced sound radiation is the result of BG-induced vibration energy redistribution over the plate and its confinement to the excitation area. This prohibits the energy from spreading out over the plate. Though a reduction in the sound radiation efficiency is not guaranteed with the BG (as in the case of a free plate), the overall weak vibration level averaged over the plate still warrants a reduced sound radiation.

The above mechanisms can be further confirmed by comparing the radiated sound power (with constant energy input) when damping layers are applied, as shown in Fig. 11. For the uniform plate, the reduction in the normalized radiation sound power is insignificant since the energy dissipation by thin damping layers is limited. In sharp contrast, a systematic and significant reduction can be observed in nearly the entire frequency range outside the BG, which demonstrates the earlier cut-on of ABH effect and the resultant accumulated energy for efficient dissipation by damping layers. Inside the BG, damping layers show little effect on the sound radiation reduction because of the vibration concentration within the small energy input area. Overall, the proposed periodic ABH plate shows prominent ability in reducing radiation sound power within ultra-broad frequency bands, especially with the help of a suitable damping treatment.

IV. EXPERIMENTAL VALIDATION

For validations, experiments were carried out on a periodic ABH plate with 6×4 cells in a semi-anechoic chamber. The cut-off frequency of the chamber is roughly 80 Hz. The plate was three-dimensionally (3D) printed using aluminum powder with a mass density of 2550 kg/m^3, Yong's modulus of 70 GPa, Poisson's ratio of 0.3, and a damping loss factor of 0.001. The structural parameters of the plate were set as $a = 80$ mm, $h = 7.2$ mm, $h_0 = 0.6$ mm, $m = 3$, $r = 15$ mm, and $l_{ABH} = 50$ mm. The experimental system is shown in Fig. 12. Through four elastic strings, the tested plate was horizontally suspended at the center of a thick wooden baffle of 2200 mm × 2200 mm × 20 mm, as shown in Fig. 12(a). Four wooden panels with 2200 mm × 600 mm × 20 mm were used to support the wooden baffle at the four edges to further reduce the sound diffraction. Gaps between the tested plate

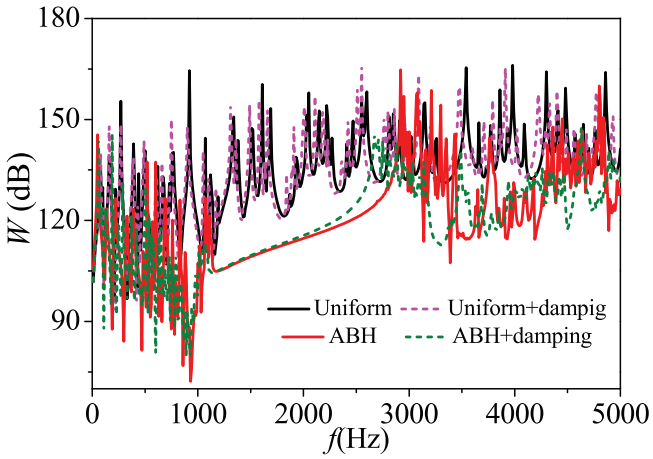

FIG. 11. (Color online) Effect of damping layers on radiated sound power per unit input power.

https://doi.org/10.1121/10.0007067

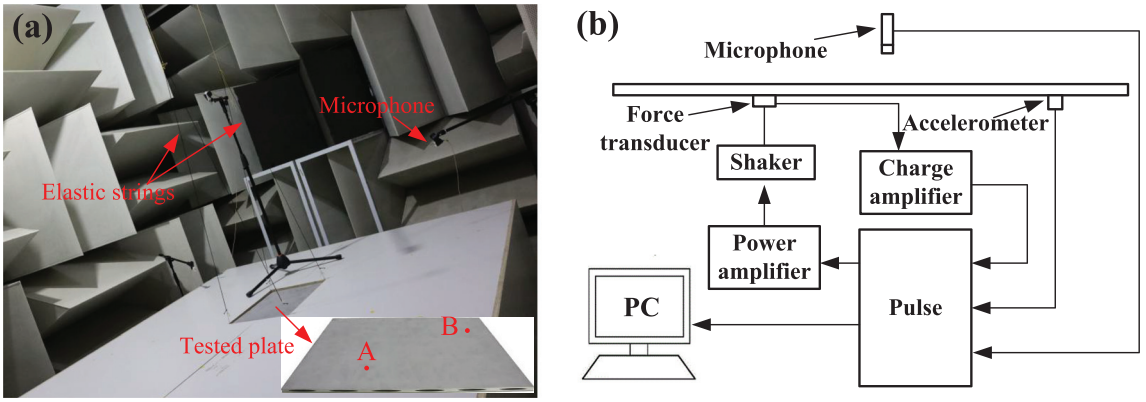

FIG. 12. (Color online) Experimental setup for radiation sound power test: (a) schematic of the test sample and installation in a semi-anechoic chamber; (b) measurement system.

and the wooden baffle are around 1.5 mm, which along with four elastic strings help achieve the free boundary conditions. As shown in Fig. 12(b), A Brüel & Kjaer Pulse system was used for signal generation and data acquisition. The generated sweep sine from 0 to 5 kHz drove an electromagnetic shaker (MB Dynamics MODAL50) after being magnified by a power amplifier, and then applied at the point A on the plate, as shown in Fig. 12(a). To minimize the background noise, the shaker was sealed inside a thick-walled box filled with sound-absorbing cotton. The excitation force was measured by a force transducer (PCB PIEZOTRONICS 208C02). The vibration acceleration was picked by an accelerometer (Brüel & Kjaer 4533b) at the point B. The radiation sound power was obtained through sound pressure measurement according to the international standard ISO 3744.[38] Twenty microphones were located over a hemisphere with a radius R of 1100 mm to measure the sound pressure level L_{pi} ($i = 1, 2,\ldots 20$). All measured data were fed back to the Pulse system for fast Fourier transform (FFT) post-processing. The radiation sound power was obtained by $L_w = \overline{L_p} + 10\lg(S/S_0)$ with $S = 2\pi R^2$ being the area of hemispherical surface, $S_0 = 1\ \mathrm{m}^2$, and $\overline{L_p}$ being the surface time-averaged sound pressure level. $\overline{L_p}$ can be obtained by $\overline{L_p} = 10\log 10(1/N\sum_i^N 10^{0.1L_{pi}}) - K_1$, where K_1 is the background noise correction, which is zero, and N is 20, respectively, in the present case.

The experimental results are presented and compared with numerical ones in Fig. 13. The measured cross-point mobility agrees reasonably well with that from numerical simulations, in terms of both peak locations and amplitude levels, especially at low frequencies. The difference at higher frequencies may be due to the local machining error of the ABH plate and the torsional modes which are ignored in the simulation. Particularly, a broad vibration attenuation band (corresponding to a strong vibration energy reduction) can be clearly seen, roughly from 2000 to 3800 Hz, showing again a consistency between experimental and numerical results. Within this attenuation band, the measured radiation sound power is also significantly reduced, also consistent with the numerical prediction. Below the attenuation band, the measured radiation sound power agrees roughly with the calculation in terms of variation tendency, although some additional peaks and differences in level are clearly observable from 800 to 2000 Hz. Nevertheless, the experiments agree reasonably well with the numerical results and thus validate the above calculation results as well as the revealed predominant sound radiation properties brought by the proposed periodic ABH plate.

V. CONCLUSIONS

As an attempt to conceive light-weight structures for better and broadband acoustic performance, this paper

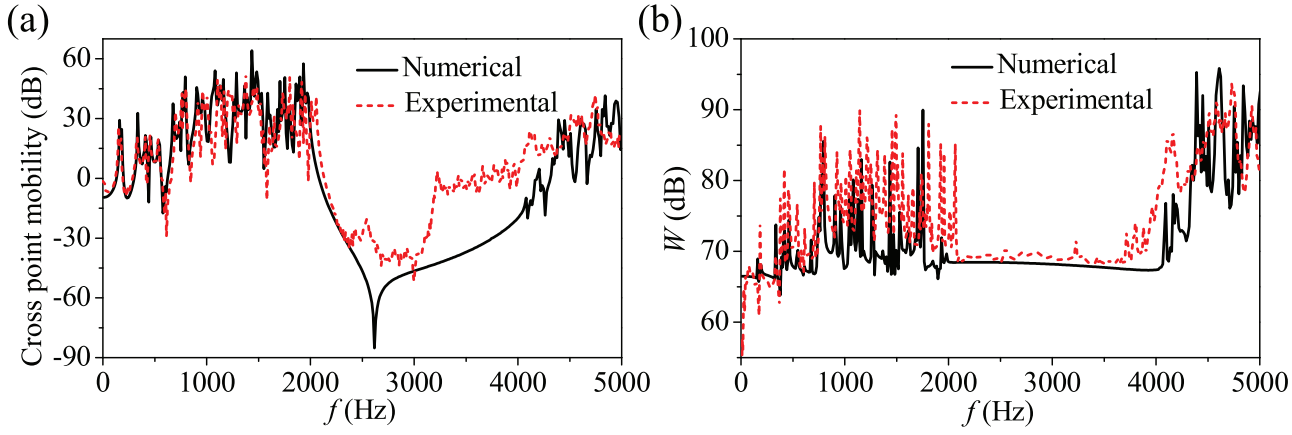

FIG. 13. (Color online) Comparisons of (a) cross-point mobility and (b) radiated sound power between the experimental and numerical results.

investigated the sound radiation properties of a tactically designed plate comprising periodically tangled double-leaf ABH cells. Through proper combination of the ABH effects and sub-wavelength BG features, the plate is shown to exhibit superior sound radiation properties in an ultra-broad frequency range, far below the cut-on frequency of the conventional ABH elements.

Analyses show that, outside the BGs, the sound radiation efficiency of the proposed plate is systematically lower than that of its uniform counterpart, which results from the tangled nature of the ABH elements to extend the actual characteristic dimension of the ABH and to lower the ABH effective frequency through creating slow waves inside the structure. The earlier onset of the ABH effects is evidenced by a systematic increase in the modal loss factors of the structure starting from low frequencies and a reduction of the sound radiation efficiency through super-to-subsonic transformation of the vibration energy, in contrast to the uniform plate with equivalent stiffness and mass. Benefiting from the low radiation efficiency, the radiated sound power under the same energy input is also systematically and significantly reduced over a broad frequency range. Inside the BGs, the vibration energy is redistributed and mainly confined within the limited excitation area. This results in a reduction in the overall vibration energy level over the plate. Consequently, even in the absence of systematic sound radiation efficiency reduction, the radiated sound power can still be significantly lower than that from the uniform plate, even without damping layers.

Some of the above phenomena are confirmed by experiments. Clearly, BGs can be tuned by changing ABH parameters to cope with targeted frequency ranges for noise reduction. Moreover, the proposed ABH design ensures the light-weight nature of the structure by tangled holes and improved stiffness by double branched facing, as compared with conventional ABH structures. Capitalizing on the combined ABH effects and BG features alongside its improved mechanical properties in structural weight and stiffness compared with conventional ABH design, the proposed ABH plate shows promise as a light-weight solution for broadband noise reduction.

ACKNOWLEDGMENTS

This work was supported by the National Science Foundation of China (Grant Nos. 11902260, 11532006, 11974287), China Postdoctoral Science Foundation (Grant No. 260456), and Research Grant Council of the Hong Kong SAR (PolyU 152017/17E).

[1]M. A. Mironov, "Propagation of a flexural wave in a plate whose thickness decreases smoothly to zero in a finite interval," Sov. Phys. Acoust. **34**(3), 318–319 (1988).
[2]V. V. Krylov and F. J. B. S. Tilman, "Acoustic 'black holes' for flexural waves as effective vibration dampers," J. Sound Vib. **274**, 605–619 (2004).
[3]D. J. O'Boy and V. V. Krylov, "Damping of flexural vibrations in circular plates with tapered central holes," J. Sound Vib. **330**, 2220–2236 (2011).
[4]V. B. Georgiev, J. Cuenca, F. Gautier, L. Simon, and V. V. Krylov, "Damping of structural vibrations in beams and elliptical plates using the acoustic black hole effect," J. Sound Vib. **330**, 2497–2508 (2011).
[5]L. L. Tang, L. Cheng, H. L. Ji, and J. H. Qiu, "Characterization of Acoustic Black Hole effect using a one-dimensional fully-coupled and wavelet-decomposed semi-analytical model," J. Sound Vib. **374**, 172–184 (2016).
[6]J. Deng, L. Zheng, P. Zeng, Y. Zuo, and O. Guasch, "Passive constrained viscoelastic layers to improve the efficiency of truncated acoustic black holes in beams," Mech. Syst. Signal Process. **118**, 461–476 (2019).
[7]T. Zhou and L. Cheng, "A resonant beam damper tailored with acoustic black hole features for broad-band vibration reduction," J. Sound Vib. **430**, 174–184 (2018).
[8]J. Y. Lee and W. Jeon, "Vibration damping using a spiral acoustic black hole," J. Acoust. Soc. Am. **141**, 1437–1445 (2017).
[9]V. V. Krylov and R. E. T. B. Winward, "Experimental investigation of the acoustic black hole effect for flexural waves in tapered plates," J. Sound Vib. **300**(1–2), 43–49 (2007).
[10]V. Denis, F. Gautier, A. Pelat, and J. Poittevin, "Measurement and modelling of the reflection coefficient of an acoustic black hole termination," J. Sound Vib. **349**, 67–79 (2015).
[11]S. Park, M. Kim, and W. Jeon, "Experimental validation of vibration damping using an Archimedean spiral acoustic black hole," J. Sound Vib. **459**, 114838 (2019).
[12]E. P. Bowyer and V. V. Krylov, "Slots of power-law profile as acoustic black holes for flexural waves in metallic and composite plates," Structures **6**, 48–58 (2016).
[13]E. P. Bowyer and V. V. Krylov, "Experimental study of sound radiation by plates containing circular indentations of power-law profile," Appl. Acoust. **88**, 30–37 (2015).
[14]S. C. Conlon and J. B. Fahnline, "Numerical analysis of the vibroacoustic properties of plates with embedded grids of acoustic black holes," J. Acoust. Soc. Am. **137**(1), 447–457 (2015).
[15]P. A. Feurtado and S. C. Conlon, "Wavenumber transform analysis for acoustic black hole design," J. Acoust. Soc. Am. **140**(1), 718–727 (2016).
[16]X. Li and Q. Ding, "Sound radiation of a beam with a wedge-shaped edge embedding acoustic black hole feature," J. Sound Vib. **439**, 287–299 (2019).
[17]L. Ma and L. Cheng, "Sound radiation and transonic boundaries of a plate with acoustic black hole," J. Acoust. Soc. Am. **145**(1), 164–172 (2019).
[18]L. Ma and L. Cheng, "Topological optimization of damping layout for minimized sound radiation of an acoustic black hole plate," J. Sound Vib. **458**, 349–364 (2019).
[19]H. L. Ji, X. D. Wang, J. H. Qiu, L. Cheng, Y. P. Wu, and C. Zhang, "Noise reduction inside a cavity coupled to a flexible plate with embedded 2-D acoustic black holes," J. Sound Vib. **455**, 324–338 (2019).
[20]X. D. Wang, H. L. Ji, J. H. Qiu, and L. Cheng, "Wavenumber domain analyses of vibro-acoustic decoupling and noise attenuation in a plate-cavity system enclosed by an acoustic black hole plate," J. Acoust. Soc. Am. **146**(1), 72–84 (2019).
[21]P. Feurtado and S. Conlon, "Transmission loss of plates with embedded acoustic black holes," J. Acoust. Soc. America **142**(3), 1390–1398 (2017).
[22]J. Deng, O. Guasch, L. Maxit, and L. Zheng, "Transmission loss of plates with multiple embedded acoustic black holes using statistical modal energy distribution analysis," Mech. Syst. Signal Process. **150**, 107262 (2021).
[23]L. L. Tang and L. Cheng, "Enhanced Acoustic Black Hole effect in beams with a modified thickness profile and extended platform," J. Sound Vib. **391**, 116–126 (2017).
[24]V. Denis, A. Pelat, C. Touzé, and F. Gautier, "Improvement of the acoustic black hole effect by using energy transfer due to geometric nonlinearity," Int. J. Nonlinear Mech. **94**, 134–145 (2017).
[25]H. Li, C. Touzé, A. Pelat, and F. Gautier, "Combining nonlinear vibration absorbers and the Acoustic Black Hole for passive broadband flexural vibration mitigation," Int. J. Nonlinear Mech. **129**, 103558 (2021).
[26]H. Li, M. Sécail-Géraud, A. Pelat, F. Gautier, and C. Touzé, "Experimental evidence of energy transfer and vibration mitigation in a vibro-impact acoustic black hole," Appl. Acoust. **182**, 108168 (2021).
[27]L. Tang and L. Cheng, "Broadband local resonant bandgaps in periodic structures with embedded acoustic black holes," J. Appl. Phys. **121**, 194901 (2017).

https://doi.org/10.1121/10.0007067

[28]L. Tang and L. Cheng, "Ultrawide band gaps in phononic beams with double-leaf acoustic black hole indentations," J. Acoust. Soc. Am. **142**(5), 2802–2807 (2017).
[29]L. Tang and L. Cheng, "Periodic plates with tunneled Acoustic-Black-Holes for directional band gap generation," Mech. Syst. Signal Process. **133**, 106257 (2019).
[30]N. Gao, Z. Wei, H. Hou, and A. O. Krushynska, "Design and experimental investigation of v-folded beams with acoustic black hole indentations," J. Acoust. Soc. Am. **145**(1), EL79–EL83 (2019).
[31]Y. Zhang, K. Chen, Y. Cheng, and Z. Wei, "Lightweight-high-stiffness vibration insulator with ultra-broad band using graded double-leaf acoustic black holes," Appl. Phys. Exp. **13**, 017007 (2020).
[32]L. Tang and L. Cheng, "Impaired sound radiation in plates with periodic tunneled Acoustic Black Holes," Mech. Syst. Signal Process. **135**, 106410 (2020).
[33]L. Tang, L. Cheng, and K. Chen, "Complete sub-wavelength flexural wave band gaps in plates with periodic acoustic black holes," J. Sound Vib. **502**, 116102 (2021).
[34]F. Fahy and P. Gardonio, *Sound and Structural Vibration: Radiation, Transmission and Response* (Elsevier, Amsterdam, 2009).
[35]E. G. Williams, "Supersonic acoustic intensity," J. Acoust. Soc. Am. **97**(1), 121–127 (1995).
[36]E. G. Williams, "Supersonic acoustic intensity on planar sources," J. Acoust. Soc. Am. **104**(5), 2845–2850 (1998).
[37]E. Fernandez-Grande, F. Jacobsen, and Q. Leclère, "Direct formulation of the supersonic acoustic intensity in space domain," J. Acoust. Soc. Am. **131**(1), 186–193 (2012).
[38]ISO 3744-2009: *Acoustic-Determination of Sound Power Levels of Noise Sources Using Sound Pressure-Engineering Method in an Essentially Free Field over a Reflecting Plane* (International Organization for Standardization, Brussels, Belgium, 2009).